Memorias del XX Congreso Latinoamericano de Control Automático (CLCA 2025)
13-17 de Octubre, 2025. Cancún, Quintana Roo, México

Cascaded Integral-Retarded Control of Switched DC-DC Boost Converters

Alejandro Martínez-González * **Luis A. Martínez** *
Adrián Ramírez *,**

* *División de Control y Sistemas Dinámicos, IPICYT, SLP, México (e-mails: alejandro.martinez@ipicyt.edu.mx)*
** *SECIHTI, CDMX (e-mail: adrian.ramirez@ipicyt.edu.mx)*

Abstract: In this paper, we explore the use of a delay-based control scheme consisting of two Integral-Retarded (IR) controllers arranged in a cascaded architecture for regulating a DC-DC boost converter. The proposed control scheme utilizes an inner-current loop that adds damping by feeding back the inductor current, and an outer-voltage loop that regulates the converter's output voltage. Specifically, both inner and outer IR controllers are designed to improve the dynamic response during load and input voltage changes while attenuating high-frequency measurement noise. Tuning formulas are derived by assigning a triple real dominant root to the closed-loop system. Simulation results show better robustness properties compared to the traditional cascaded Proportional-Integral (PI) control scheme, showing the effectiveness of the delay-based approach.

Keywords: Boost Converters, Delay-based Control, Cascaded Control.

1. INTRODUCTION

The increasing need for efficient and reliable power conversion across various applications calls for advanced control strategies in DC-DC power converters (Severns and Bloom, 1985). In this context, PI controllers have been traditionally adopted due to their simplicity and robustness; however, they often struggle to deliver fast dynamic responses, especially in systems with complex dynamics or fluctuating operating conditions (Ogata, 2010; Guo et al., 2009). Among DC-DC power converters, boost topologies are fundamental components widely used in power electronics to step up a low input voltage to a high output voltage, with the advantage of maintaining precise regulation under varying load and source conditions (Severns and Bloom, 1985). Nevertheless, designing controllers for boost converters is challenging due to their inherent complexities and well-known non-minimum phase behavior, which can limit performance in terms of disturbance rejection, and transient and steady-state responses (Middlebrook and Ćuk, 1976).

To address these challenges, delay-based controllers, such as Integral-Retarded (IR) controllers, have emerged as a promising alternative. By intentionally introducing time delays in the feedback loop, IR controllers provide improved robustness and performance compared to traditional approaches (Fossas and Olivar, 1996; Ramírez et al., 2020). While delay-based control has been successfully applied to buck converters in a single-loop configuration (Ramírez et al., 2020), its application to the more challenging boost converter remains largely unexplored. To overcome the limitations of single-loop control, cascaded architectures have been widely adopted, typically employing PI controllers in an inner-current loop and an outer-voltage loop, which allows independent tuning and significantly improves stability margins and dynamic performance (Severns and Bloom, 1985; Guo et al., 2009). Building on this concept, this paper proposes a *cascaded IR control strategy* for boost converters, combining the robustness of delay-based design with the flexibility of a cascaded structure to improve transient performance, disturbance rejection, and noise attenuation.

By integrating time delays within a cascaded control framework, the proposed IR controller harnesses its structural simplicity to achieve faster settling times and enhanced disturbance rejection while avoiding the high-frequency noise amplification often observed in traditional controllers (Fossas and Olivar, 1996; Ramírez et al., 2020; Niculescu and Sipahi, 2012). This design ensures that the boost converter operates in a stable, efficient, and high-performance manner, effectively addressing the challenges inherent to this topology.

2. PRELIMINARIES

State-space averaging is a widely accepted technique for modeling DC-DC converters due to its accuracy and simplicity (Middlebrook and Ćuk, 1976). The standard small-signal model is derived through a procedure that involves three key steps. First, it involves developing a switched model that precisely captures the converter's behavior, considering its discrete switching states. Second, the state averaging technique is applied to obtain a continuous-time averaged model, which simplifies the analysis of the converter's dynamics. Finally, the averaged model is linearized around a steady-state operating condition to obtain the small-signal model. This approach offers several advantages, such as a clear and simple representation of the converter dynamics, facilitating controller design. The

https://doi.org/10.58571/CNCA.AMCA.2025.029

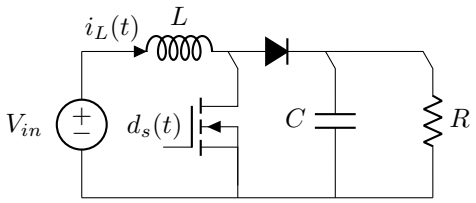

Fig. 1. DC-DC boost converter feeding a resistive load R.

averaged model of the boost converter, shown in Fig. 1 is then given by

$$\frac{di_L}{dt} = \frac{1}{L}\Big[V_{in} - (1-d)v_o\Big], \tag{1}$$

$$\frac{dv_o}{dt} = \frac{1}{C}\Big[(1-d)i_L - \frac{v_o}{R}\Big], \tag{2}$$

where i_L is the current flowing through the inductor L and v_o is the voltage across the terminals of the capacitor C. The steady-state relationships $V_o = V_{in}/(1-D)$ and $I_L = V_o/(R(1-D))$, where V_{in} is the input voltage, D is the nominal value duty cycle $d(t) \in [0,1]$, and R the load resistance. The *small-signal* representation on the above averaged model is given by

$$\frac{d\hat{i}_L}{dt} = \frac{1}{L}\Big[-(1-D)\hat{v}_o + \frac{V_{in}}{1-D}\hat{d}\Big], \tag{3}$$

$$\frac{d\hat{v}_o}{dt} = \frac{1}{C}\Big[(1-D)\hat{i}_L - \frac{1}{R}\hat{v}_o - \frac{V_{in}}{R(1-D)^2}\hat{d}\Big], \tag{4}$$

where $\hat{i}_L$, $\hat{v}_o$ and $\hat{d}$ are respectively, the small-signal inductor current, small-signal output voltage, and small-signal duty cycle. Although the state-space averaging technique provides a simple framework for controller design, it is important to note its limitations. For instance, the model's accuracy can be sensitive to parametric variations, like component tolerances or significant load changes.

3. IR CONTROL OF THE BOOST CONVERTER

The limitations of single-loop control boost converters, particularly the challenges posed by their non-minimum phase behavior, motivate the adoption of cascaded control architectures to achieve robust performance and stability.

3.1 Cascaded Control Design

The proposed cascaded control scheme, as depicted in Fig. 2, is designed under a common assumption, namely, the inner-current loop operates significantly faster than the outer-voltage dynamics. Consequently, during the current loop's operation, the output voltage is considered approximately constant.

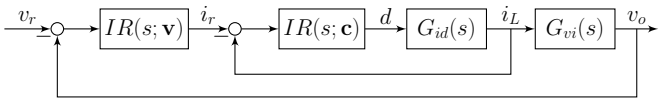

Fig. 2. Proposed double-loop cascaded control scheme.

Under this assumption, the small-signal control-to-current transfer function for the inner loop, $G_{id}(s) = \hat{i}_L(s)/\hat{d}(s)$, can be derived from the small-signal model by neglecting the influence of $\hat{v}_o$ on $\hat{i}_L$ dynamics, leading to

$$G_{id}(s) = \frac{V_{in}}{(1-D)Ls}. \tag{5}$$

The rapid dynamics of the inner-current loop ensure its effective regulation of the inductor current. This current regulation mitigates the direct influence of the small-signal duty cycle variation, $\hat{d}$, on the voltage dynamics when analyzing the outer loop. Hence, for the design of the outer-voltage controller, the term associated with $\hat{d}$ in the small-signal voltage equation can be neglected. This simplification allows us to obtain the small-signal current-to-voltage transfer function for the outer loop, $G_{vi}(s) = \hat{v}_o(s)/\hat{i}_L(s)$, as follows

$$G_{vi}(s) = \frac{(1-D)R}{RCs+1}. \tag{6}$$

Having established these small-signal transfer functions, $G_{id}(s)$ and $G_{vi}(s)$, the next step is to design the controllers. The main contribution of this work is the application of a control strategy based on intentional time delays, utilizing Integral-Retarded (IR) controllers.

The general form of the IR controller, parameterized by the vector $\mathbf{p} = (h, k_i, k_r)$, is given by

$$IR(s;\mathbf{p}) = \frac{k_i - k_r e^{-hs}}{s}. \tag{7}$$

This controller is employed in both the inner-current loop and the outer-voltage loop. Specifically, the inner-current loop is controlled by $IR(s;\mathbf{c})$, where the parameter vector is $\mathbf{c} = (h_v, k_{ic}, k_{rc})$, providing fast control over the inductor current. This allows the outer-voltage loop, controlled by $IR(s;\mathbf{v})$ with parameter vector $\mathbf{v} = (h_v, k_{iv}, k_{rv})$, to maintain the output voltage at the desired level despite sudden changes in load.

3.2 IR Cascaded Controller Tuning

The design of the cascaded IR controllers begins with the inner-current loop. The goal is to achieve a desired exponential decay rate, γ_c, ensuring the fast response previously assumed. This problem is approached by imposing the maximal exponential decay rate on the inner closed-loop system.

Considering the IR controller $IR(s;\mathbf{c})$ as in (7) and $G_{id}(s)$ as in (5), the associated characteristic function results in

$$f_c(s) = (1-D)Ls^2 + V_{in}k_{ic} - V_{in}k_{rc}e^{-h_c s}. \tag{8}$$

In (Villafuerte et al., 2013; Ramírez et al., 2015; Ramírez et al., 2017), the authors characterize the point of maximum exponential decay as the collapsing of the stability region in the parameter space (h, k_i, k_r) into a point, which is associated with a triple real root $s = -\gamma$ of the characteristic function. While γ is a design choice, the stability of the closed-loop system is guaranteed for variations in the designed parameters.

The maximum exponential decay is achieved when the characteristic function $f_c(s)$ in (8) has a triple real root at $s = -\gamma_c$. This condition can be found by shifting the characteristic function by $f_c(s-\gamma_c)$ and imposing a triple real root at $s = 0$. The conditions for this are $f_c(s-\gamma_c) = \partial f_c(s-\gamma_c)/\partial s = \partial^2 f_c(s-\gamma_c)/\partial s^2 = 0$, evaluated at $s = 0$. These conditions can be expressed as follows

 https://doi.org/10.58571/CNCA.AMCA.2025.029

$$V_{in}k_{rc}e^{\gamma_c h_c} = L\gamma_c^2 + V_{in}k_{ic}, \tag{9}$$
$$h_c V_{in}k_{rc}e^{\gamma_c h_c} = 2L\gamma_c, \tag{10}$$
$$h_c^2 V_{in}k_{rc}e^{\gamma_c h_c} = 2L. \tag{11}$$

Solving simultaneously the system of equations (9), (10) and (11), we can obtain explicit expressions for h_c, k_{ic} and k_{rc} that establish γ_c as the maximum exponential decay rate. It can be easily seen that dividing (11) by (10) yields

$$h_c = \frac{1}{\gamma_c}.$$

By performing further algebraic manipulations from the system of equations, such as dividing (10) by (9) and (11) by (9) and then eliminating h_c, the equations can be reduced to a simpler form that determines an expression for k_{ic} which is given by

$$L\gamma_c^2 - V_o k_{ic} = 0.$$

The same procedure is applied to the outer-voltage loop. Considering the IR controller $IR(s;\mathbf{v})$ as in (7) and $G_{vi}(s)$ as in (6), the associated characteristic function is given by:

$$f_v(s) = RCs^2 + s + (1-D)Rk_{iv} - (1-D)Rk_{rv}e^{-h_v s}. \tag{12}$$

The equations that result from the triple root at $-\gamma_v$ for $f_v(s-\gamma_v)$ are given by

$$RV_{in}k_{rv}e^{\gamma_v h_v} = CRV_o\gamma_v^2 + RV_{in} - V_o\gamma_v, \tag{13}$$
$$h_v RV_{in}k_{rv}e^{\gamma_v h_v} = V_o(2CR\gamma_v - 1), \tag{14}$$
$$h_v^2 RV_{in}k_{rv}e^{\gamma_v h_v} = 2CRV_o. \tag{15}$$

In the same manner as the system of equations for the inner-current loop was simplified, we can reduce equations (13), (14) and (15) to the following expressions:

$$h_v = \frac{2CR}{2CR\gamma_v - 1},$$
$$0 = 2C^2R^2V_o\gamma_v^2 - 2CR^2V_{in}k_{iv} - 2CRV_o\gamma_v + V_o.$$

The derived tuning procedure for each loop ensures that the dominant roots are placed to guarantee a maximum decay rate γ, thus providing a robust performance. This analytical approach allows for the direct computation of the control parameters in both inner and outer loops to achieve a predefined γ. This optimization yields explicit relationships between the system parameters and the controller gains.

Proposition 1. Consider the boost converter operating under a cascaded IR control architecture, where both inner-current and outer-voltage loops employ controllers of the form $IR(s;\mathbf{p})$, for a reference output voltage V_r.

- *Inner-Current Loop.* If the parameters of the inner-current controller, $IR(s;\mathbf{c})$, for the small-signal transfer function $G_{id}(s)$ as in (5), are tuned according to:

$$h_c = \frac{1}{\gamma_c}, \tag{16}$$
$$k_{ic} = \frac{(1-D)L}{V_{in}}\gamma_c^2, \tag{17}$$
$$k_{rc} = \frac{2(1-D)L}{V_{in}e}\gamma_c^2. \tag{18}$$

- *Outer-Voltage Loop.* Similarly, if the parameters of the outer-voltage controller, $IR(s;\mathbf{v})$, for the small-signal transfer function $G_{vi}(s)$ as in (6), are tuned by:

$$h_v = \frac{2CR}{2CR\gamma_v - 1}, \tag{19}$$
$$k_{iv} = \frac{V_r\left(2C^2R^2\gamma_v^2 - 2CR\gamma_v + 1\right)}{2CR^2V_{in}}, \tag{20}$$
$$k_{rv} = \frac{V_r\left(4C^2R^2\gamma_v^2 - 4CR\gamma_v + 1\right)}{2CR^2V_{in}}e^{-\frac{2CR\gamma_v}{2CR\gamma_v - 1}}, \tag{21}$$

then both the inner-current and outer-voltage loops are exponentially stable, with a decay rate of γ_c.

The preceding proposition establishes the robust local asymptotic stability and desired transient performance of each individual control loop. From these results, the following proposition addresses the stability of the complete cascaded system.

Proposition 2. Consider the boost converter, described by its averaged non-linear model (1)-(2), operating under the cascaded IR control architecture. If $\gamma_c > \gamma_v$, and the inner-current controller (IR, c) and the outer-voltage controller (IR, v) are tuned according to (17)-(18)-(19) and (16)-(20)-(21) respectively, then the equilibrium point (I_L^*, V_O^*) of the closed-loop system is exponentially stable.

This analytical framework provides explicit tuning rules for the cascaded IR controllers, guaranteeing desired transient respond and robust stability for the boost converter. To evaluate the advantages of the proposed IR controllers, a conventional PI control strategy is also implemented and compared under the same operating conditions.

3.3 PI Cascaded Controller Tuning

For the purpose of performance comparison, a conventional cascaded Proportional-Integral (PI) control strategy was also implemented with general form given by

$$PI(s;\tilde{\mathbf{p}}) = \frac{k_p s + \tilde{k}_i}{s}. \tag{22}$$

Similar to the proposed IR architecture, the PI control scheme also utilizes a cascaded structure with an inner-current loop and an outer-voltage loop. The parameters of both controllers were tuned to achieve response comparable to that of the IR controller. For the inner loop, the PI controller is defined by the parameter vector $\tilde{\mathbf{c}} = (k_{pc}, \tilde{k}_{ic})$. The characteristic function for this loop, considering the transfer function $G_{id}(s)$, is given by

$$\tilde{f}_c(s) = Ls^2 + V_o k_{pc}s + V_o k_{ic}.$$

Similarly, for the outer-voltage loop, the PI controller is defined by $\tilde{\mathbf{v}} = (k_{pv}, \tilde{k}_{iv})$, and its characteristic function with $G_{vi}(s)$ is

$$\tilde{f}_v(s) = CRV_o s^2 + (RV_{in}k_{pv} + V_o)s + RV_{in}\tilde{k}_{iv}.$$

To tune the controllers, we assign a double real root at $s = -\gamma_c$ for the inner loop characteristic function $\tilde{f}_c$, and at $s = -\gamma_v$ for the outer loop's $\tilde{f}_v$. This approach allows us to solve for the control parameters. The parameters for both the inner-current and outer-voltage controllers are tuned as follows.

 https://doi.org/10.58571/CNCA.AMCA.2025.029

- *Inner-Current Loop:*

$$k_{pc} = \frac{2L}{V_r}\tilde{\gamma}_c, \tag{23}$$

$$\tilde{k}_{ic} = \frac{L}{V_r}\tilde{\gamma}_c^2. \tag{24}$$

- *Outer-Voltage Loop:*

$$k_{pv} = \frac{V_r}{RV_{in}}\left(2CR\tilde{\gamma}_v - 1\right)\tilde{\gamma}_v, \tag{25}$$

$$\tilde{k}_{iv} = \frac{CV_r}{V_{in}}\tilde{\gamma}_v^2. \tag{26}$$

In order to make the comparison fair, the PI controllers are tuned such that their performance, characterized by the $\tilde{\gamma}_c$ and $\tilde{\gamma}_v$ rates, is comparable to that of the proposed IR control. This allows for a fair evaluation of the strengths of both control strategies over various operating conditions discussed in the simulation section.

4. SIMULATIONS

This section illustrates the main features of the proposed IR controller and compares its performance to that of a conventional PI controller. A comparator modulates the control signal using a ramp function as the PWM carrier waveform. The electronic switch is operated utilizing a gate driver, which receives the logic pulses generated by the comparator and produces the discrete switched signal $d_s(t) = \{0, 1\}$. In addition, performance is quantified using the Integral of Square of Error (ISE) and the Total Variation of Control (TVC):

$$ISE = \int_0^\infty e^2(t)dt, \quad TVC = \int_0^\infty \left|\frac{du(t)}{dt}\right| dt.$$

It is worth noting that implementing a delay-based controller in digital hardware requires approximating the delay element e^{-hs}, with delay time h as a multiple of the sampling period. A high sampling rate is needed for the desired transient response, and computational latency must also be considered. Despite these challenges, the IR controller's simplicity makes it appealing for implementation. All simulations are performed in PSIM, and the nominal parameter values used for the boost converter are given in Table 1.

4.1 Load Variations

First, the performance of the IR controller under varying load conditions is evaluated. Figure 3 illustrates the output voltage regulation as it reaches the desired reference V_r, followed by its response to periodic load variations. The desired output voltage is $V_r = 48V$ with an input voltage $V_{in} = 24$. The load periodically changes from $R = 2.88\Omega$ to $R = 5.76\Omega$ starting at time $0.02s$. In the same figure we also include the corresponding control signal (duty cycle d). This simulation aims to demonstrate the IR controller's ability to maintain robust output voltage regulation and manage power delivery efficiently under load changes. For comparative purposes, a conventional cascaded PI controller, tuned to achieve comparable transient response, is also simulated under the same operating conditions. Figure 4 shows the PI controller's performance during load variations, allowing for a direct comparison with Fig. 3.

Table 1. Boost Converter's Parameters

Nominal load (R)	5.76	Ω
Capacitor (C)	173.6	μF
Inductor (L)	40	μH
Power (P)	400	W

4.2 Measurement Noise

Next, the robustness of the IR controller to measurement noise is evaluated. Figure 5 illustrates the output voltage response v_o when a high-frequency chirp noise is introduced to the system after it reaches steady state. The behavior of the control signal d is also shown. This highlights the IR controller's inherent capability to handle such disturbances without excessively amplifying the noise in the control signal, which is a common and undesirable characteristic of traditional control methods.

As in the case of the IR controller, Fig. 6 illustrates the PI controller's response to the injected chirp noise, mirroring the scenario in Fig. 5. The tuning formulas for the cascaded PI controller, as presented (23)-(26), were derived based on this same cascaded structure to match the transient performance characteristics of the proposed cascaded IR controller. This approach validates our conclusion that the enhanced performance of the IR scheme is a result of its delay-based structure.

Table 2 shows the comparative performance of the IR and PI controllers, quantified by ISE and TVC metrics. Table 2 clearly shows that the IR control signal has fewer high-frequency components (lower TVC) than the PI control signal. Additionally, the IR controller achieves better overall performance, as indicated by its lower ISE values. These comparative figures facilitate a comprehensive evaluation of the IR controller's benefits, focusing on the control effort under load disturbances and measurement noise. The analysis highlights the IR controller's enhanced capability to deliver a cleaner control signal while ensuring robust and efficient performance.

5. CONCLUSION

This paper presents a cascaded IR control approach for DC-DC boost converters, with the goal of improving dynamic performance and robustness. The proposed IR controller improves performance without amplifying high-frequency noise. The results show that, compared to standard PI control, our approach offers robustness to load variations, immunity to measurement noise, and reduced control effort. This confirms the effectiveness of delay-based strategies in addressing control challenges of boost converters. Moreover, its simplicity and ease of tuning make it suitable for a wide range of real-world applications, including photovoltaic systems, battery charging, and electric vehicle power management.

Table 2. Performance Indices

Controller	ISE	TVC
IR Cascaded	0.387245	0.000077
PI Cascaded	0.935821	0.000921

 https://doi.org/10.58571/CNCA.AMCA.2025.029

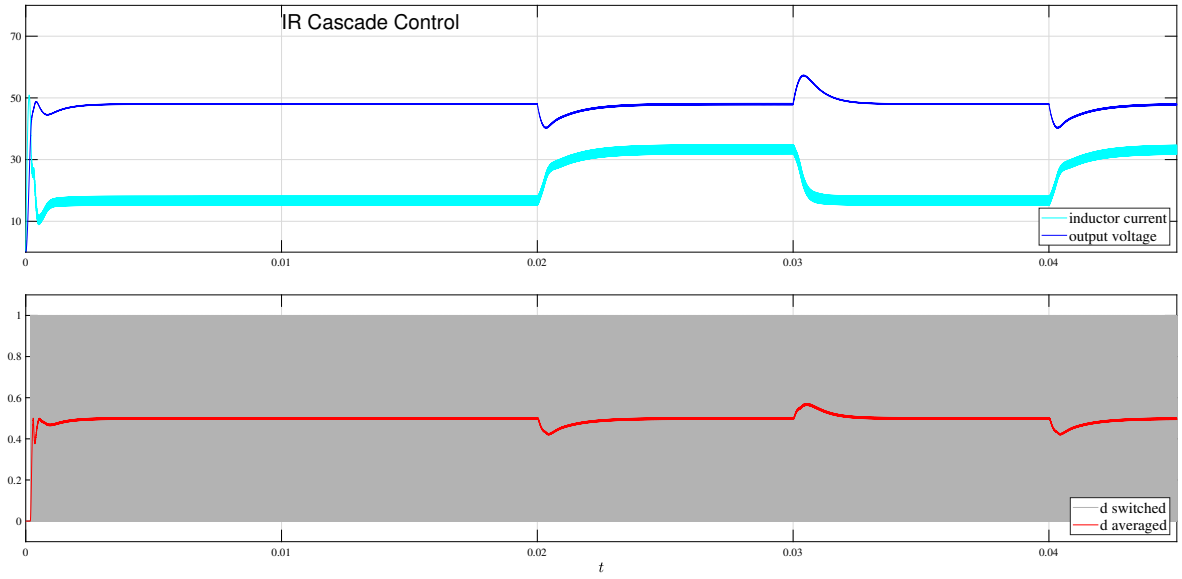

Fig. 3. Closed-loop response using the cascaded IR controller (7) under load variations. The control signal generated by the controller, denoted as the duty cycle d, is also presented, showing its averaged representation for continuous signals and its switched form for the PWM-generated signals.

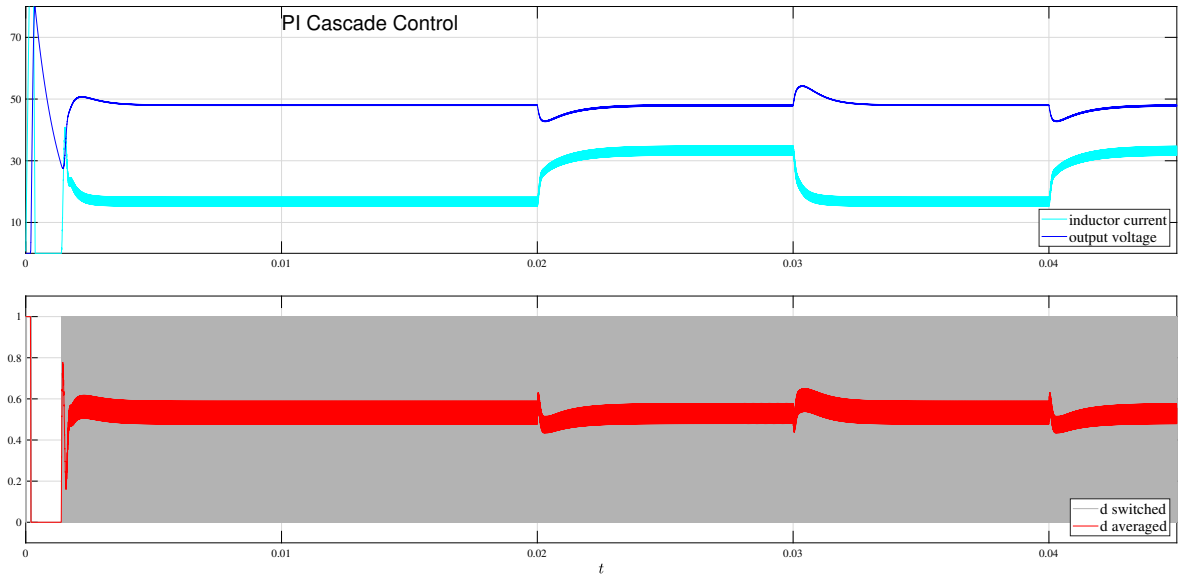

Fig. 4. Closed-loop response using the cascaded PI controller (22) under load variations. The control signal generated by the controller, denoted as the duty cycle d, is also presented, showing its averaged representation for continuous signals and its switched form for the PWM-generated signals.

REFERENCES

Fossas, E. and Olivar, G. (1996). Study of chaos in the buck converter. *IEEE Transactions on Circuits and Systems I: Fundamental Theory and Applications*, 43(1), 13–25.

Guo, L., Hung, J.Y., and Nelms, R.M. (2009). Evaluation of dsp-based pid and fuzzy controllers for dc–dc converters. *IEEE Transactions on Industrial Electronics*, 56(6), 2237–2248.

Middlebrook, R.D. and Ćuk, S. (1976). A general unified approach to modelling switching-converter power stages. *IEEE Power Electronics Specialists Conference*, 18–34.

Niculescu, S.I. and Sipahi, R. (2012). Delay effects in control systems: A new paradigm. *European Journal of Control*, 18(3), 217–218.

Ogata, K. (2010). *Modern Control Engineering*. Prentice Hall, Boston, 5 edition.

Ramírez, A., Mondié, S., Garrido, R., and Sipahi, R. (2015). Design of proportional-integral-retarded (PIR) controllers for second-order LTI systems. *IEEE Transactions on Automatic Control*, 61(6), 1688–1693.

Ramírez, A., Sipahi, R., Mondié, S., and Garrido, R. (2017). An analytical approach to tuning of delay-based controllers for LTI-SISO systems. *SIAM Journal*

 https://doi.org/10.58571/CNCA.AMCA.2025.029

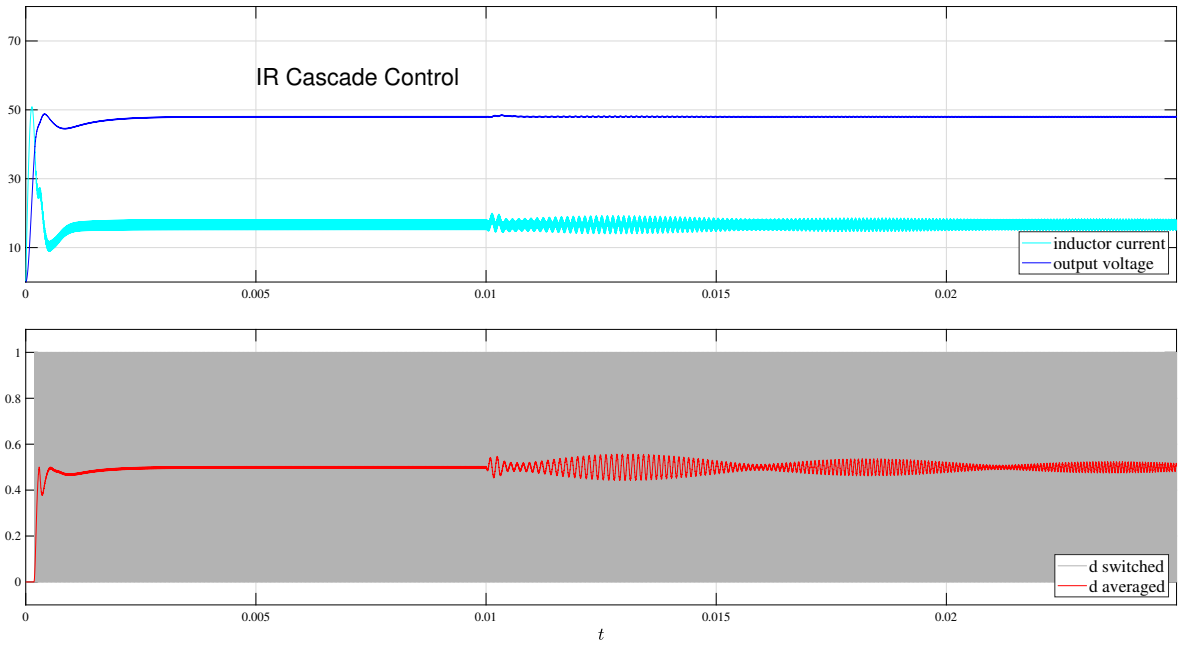

Fig. 5. Closed-loop response of the boost converter using the cascaded IR controller (7) under measurement noise. The figure shows the output voltage v_o and the corresponding control signal d generated by the controller in response to a chirp disturbance applied to the measurement.

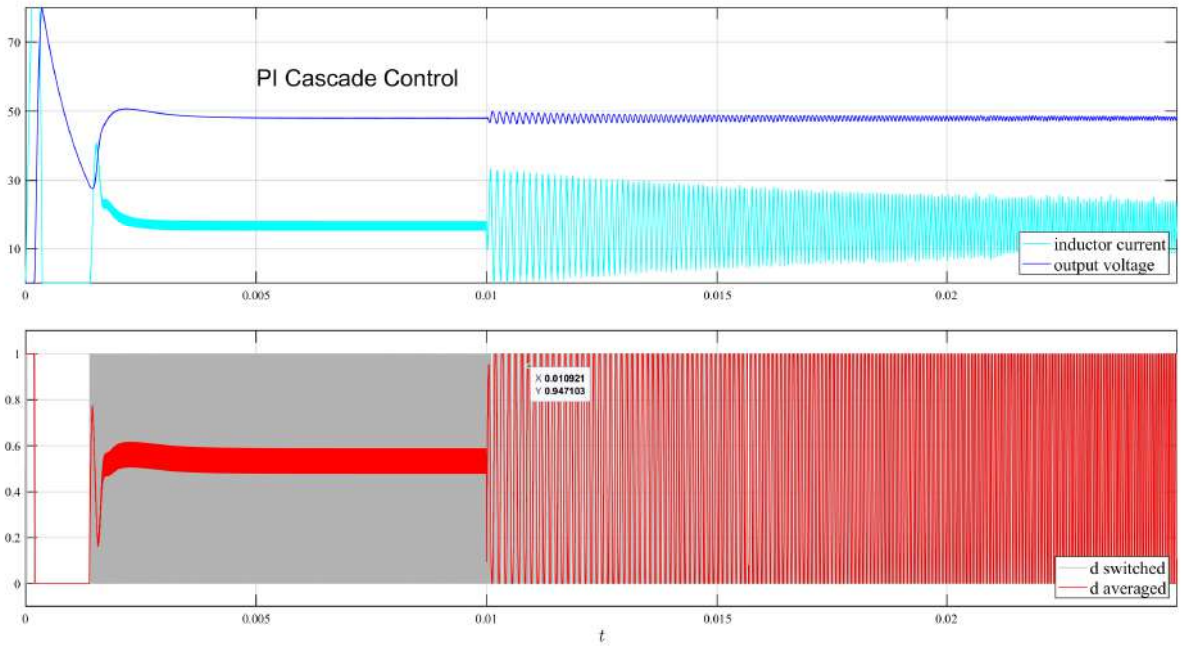

Fig. 6. Closed-loop response of the boost converter using the cascaded PI controller (22) under measurement noise. The figure shows the output voltage v_o and the corresponding control signal d generated by the controller in response to a chirp disturbance applied to the measurement.

on Control and Optimization, 55(1), 397–412. doi: 10.1137/15M1050999.

Ramírez, A., Sipahi, R., Díaz, L., and Leyva, J. (2020). Delay-based voltage-mode control of switched dc-dc buck converters for fuel-cell power applications. In *2020 7th International Conference on Control, Decision and Information Technologies (CoDIT)*, volume 1, 364–369.

Severns, R.P. and Bloom, G.E. (1985). *Modern DC-to-DC Switchmode Power Converter Circuits*. Van Nostrand Reinhold, New York.

Villafuerte, R., Mondié, S., and Garrido, R. (2013). Tuning of proportional retarded controllers: Theory and experiments. *IEEE Transactions on Control Systems Technology*, 21(3), 983–990.

 https://doi.org/10.58571/CNCA.AMCA.2025.029